Modeling scanning tunneling spectra of $Bi_2Sr_2CaCu_2O_{8+\delta}$

B. W. Hoogenboom,* C. Berthod, M. Peter,† and Ø. Fischer
DPMC, Université de Genève, 24 Quai Ernest-Ansermet, 1211 Genève 4, Switzerland

A. A. Kordyuk
Institute for Solid State Research, IFW Dresden, P.O. Box 270016, D-01171 Dresden, Germany
and Institute of Metal Physics of The National Academy of Sciences of Ukraine, 03142 Kyiv, Ukraine
(Received 13 December 2002; published 10 June 2003)

Recent angle-resolved photoemission spectroscopy (ARPES) and neutron scattering data have provided ingredients for the interpretation of scanning tunneling spectra on $Bi_2Sr_2CaCu_2O_{8+\delta}$. We analyze the low-temperature tunneling spectra, from oxygen overdoped to underdoped samples, including details about the bilayer splitting and the neutron resonance peak. Two van Hove singularities are identified: the first is integrated in the coherence peaks, the second is heavily broadened at higher binding energy. The shape of the tunneling spectra suggests a strong coupling of the quasiparticles with a collective mode, and a comparison with photoemission shows that the scattering rate in tunneling is an order of magnitude smaller than in ARPES. Finally, the theoretical spectra calculated with an isotropic tunneling matrix element are in better agreement with the experimental data than those obtained with anisotropic matrix elements.

DOI: 10.1103/PhysRevB.67.224502 PACS number(s): 74.50.+r, 73.40.Gk, 74.72.−h, 74.72.Hs

I. INTRODUCTION

Scanning tunneling spectroscopy (STS) is a powerful tool to study the electronic properties of solids. Its remarkable energy and spatial resolution makes it particularly well suited for materials characterized by small energy and short length scales, like the cuprate high-T_c superconductors (HTS). Among the HTS, the bilayer compound $Bi_2Sr_2CaCu_2O_{8+\delta}$ (BSCCO) has often been studied by STS, because it cleaves easily and offers an atomically flat BiO surface. It is possible to tunnel through the insulating BiO and SrO surface layers into the CuO_2 plane, where all the exciting properties of the cuprates are believed to reside. Many important results on the nature of the superconducting, normal, and mixed state of BSCCO have been obtained using STS.[1–8]

In the superconducting state, the main feature of the differential tunneling conductance (dI/dV) spectrum is the quasiparticle excitation gap, which has been observed in BSCCO and studied as a function of doping and temperature.[1,2,9–11] The presence of excitations within the superconducting gap, linearly increasing with energy around $V=0$, indicates that the order parameter has nodes, and presumably $d_{x^2-y^2}$ symmetry. Other characteristics of the BSCCO spectra are the celebrated dip-hump structure at energies larger than the excitation gap, an asymmetry between electron and hole tunneling, and coherence peaks with considerably more spectral weight than predicted by BCS theory. None of these three characteristics has been met with an explanation that is commonly agreed upon.

Under certain assumptions,[12,13] and considering the nearly two-dimensional nature of BSCCO, one finds that the shape of the STS spectrum is determined by only three ingredients: the bare electron dispersion $\varepsilon_{\boldsymbol{k}}$ in the CuO_2 plane, the self-energy $\Sigma(\boldsymbol{k},\omega)$ which embodies all electronic interactions, and a tunneling matrix element $T_{\boldsymbol{k}}$ which couples the electronic states of momentum $\boldsymbol{k}$ at the sample surface with the metallic tip. In the particular case where $T_{\boldsymbol{k}}$ is a constant, the STS spectrum directly relates to the quasiparticle density of states (DOS) in the CuO_2 plane. Behind this apparently simple statement lies a real difficulty to disentangle the contribution of each of the above ingredients. Various features in the STS spectra were thus attributed either to van Hove singularities in the band-structure[14,15] or to self-energy effects.[16,17] Furthermore, the general shape of the low-temperature spectrum was considered suggestive of an anisotropic matrix element.[15,18–20]

The situation has recently become even more complicated with the observation of a clear bilayer splitting by angle-resolved photoemission (ARPES).[21–23] The two CuO_2 layers in the BSCCO unit cell give rise to two non-degenerate bands close to the Fermi energy. As a consequence, there are two bands — instead of one, as assumed previously — which can contribute to the dI/dV spectra. Using ARPES, the shape of these bands has been determined in the normal state of underdoped and overdoped BSCCO.[24]

In fact, the correct interpretation of STS spectra relies upon a realistic modeling of the data, and different models can lead to opposite conclusions. Moreover, the modeling critically depends on details of the band structure[24] and of the spin excitation spectrum,[25,26] which have become available only very recently.

In this study we compare the predictions of several models to the STS spectra measured at low temperature on BSCCO samples with different oxygen dopings levels.[1] Our calculations take into account the bilayer splitting and are based on the band structures determined in Ref. 24. We assume a pure $d_{x^2-y^2}$ symmetry of the superconducting gap and consider three different models for the self-energy: a conventional BCS model; a phenomenological model proposed to fit the ARPES data,[24] thus allowing a direct comparison between photoemission and tunneling; and a model which describes the coupling of quasiparticles to a collective mode.[27] The latter model takes into account some aspects similar to conventional strong-coupling theory, leading to ad-

ditional structure in the tunneling spectra at higher energies (but neglecting the possibly complex and energy-dependent nature of the superconducting gap). We also compare the effects of isotropic and anisotropic tunneling matrix elements.

Many of the topics raised in this work probably apply to other HTS as well. However, we restrict this study to BSCCO, since we feel that only for BSCCO the tunneling and ARPES data have been defined, elaborated and established in sufficient detail to serve for the quantitative analysis below.

II. MODELING THE TUNNELING SPECTRA

In the tunneling-Hamiltonian formalism,[12] the sample and tip are coupled by a matrix element $M_{\boldsymbol{kq}}$ which represents the overlap of the electronic states on both sides of the tunnel junction. The resulting differential conductance at bias voltage V is given by

$$\frac{dI}{dV} \propto -\int d\omega \sum_{\boldsymbol{k},n} |T_{\boldsymbol{k}}|^2 A_n(\boldsymbol{k},\omega) f'(\omega - eV) \tag{1}$$

where f is the Fermi function and A_n is the spectral function in the sample. The sign convention is such that, at zero temperature, negative energies ω and eV correspond to occupied states, and positive energies to unoccupied states. The new matrix element appearing in Eq. (1) is $|T_{\boldsymbol{k}}|^2 = \Sigma_{\boldsymbol{q}} |M_{\boldsymbol{kq}}|^2 A_{\mathrm{tip}}(\boldsymbol{q},\omega)$. Using a tip with a featureless DOS, we can assume that it is energy independent. According to Ref. 13 the dependence of $T_{\boldsymbol{k}}$ on k_z is cancelled by the band dispersion along k_z (z is the tunneling direction). In Eq. (1), n refers to the two bands resulting from the bilayer splitting as discussed below. We assume that the k_{xy} dependence of $T_{\boldsymbol{k}}$ is the same for both bands; this then leads to an n-independent matrix element. A_n is related to the electron dispersion and self-energy through

$$A(\boldsymbol{k},\omega) = -\frac{1}{\pi} \mathrm{Im}\left[\frac{1}{\omega + i\Gamma - \varepsilon_{\boldsymbol{k}} - \Sigma(\boldsymbol{k},\omega)}\right]. \tag{2}$$

The band index is omitted for simplicity. The lifetime broadening Γ is introduced here for computational convenience and is set to $\Gamma = 1$ meV in all of our calculations.

To account for the bilayer splitting, we use the band structures determined in Ref. 24 for the anti-bonding (A, plus sign) and bonding (B, minus sign) bands:

$$\varepsilon_{\boldsymbol{k}}^{(\mathrm{A,\,B})} = -2t(\cos k_x + \cos k_y) + 4t' \cos k_x \cos k_y - 2t''(\cos 2k_x + \cos 2k_y) \pm \tfrac{1}{4} t_\perp (\cos k_x - \cos k_y)^2 + \Delta\varepsilon. \tag{3}$$

The interlayer coupling is described by $t_\perp$; the maximum energy splitting between the A and B bands is $2t_\perp$ and coincides with the van Hove singularities at the $(\pi,0)$ point in the Brillouin zone. It is worth pointing out that the van Hove singularities of the two-dimensional band structure $\varepsilon_{\boldsymbol{k}}$ of BSCCO are expected to show up in the tunneling spectra,[15,20] in contrast to the case of tunneling into more three-dimensional materials.[13] The tight-binding parameters inferred from ARPES for overdoped (OD69.0K) and underdoped (UD77.0K) BSCCO are given in Table I. These parameters deviate slightly from those reported in Ref. 24. $t_\perp$ was determined in Ref. 24 for the OD69.0K sample. The determination of $t_\perp$ for the UD77.0K sample is complicated by the strong influence of the pseudo- and superconducting gaps on the photoemission spectra. For that reason, UD77.0K was assumed to have the same $t_\perp$ as OD69.0K in Ref. 24. In this work, we have estimated $t_\perp$ for UD77.0K from a careful comparison between leading edge gaps of the A and B bands.[28] The remaining parameters were modified accordingly. This leads to a better agreement with the tunneling data. From the parameters of OD69.0K and UD77.0K, we make a linear interpolation with doping to obtain the parameters appropriate for the samples studied by STS (Table I).[29]

TABLE I. Tight-binding parameters for the conduction bands of BSCCO. The parameters for OD69.0K and UD77.0K follow from fits to ARPES data, and in the other cases from a linear interpolation with doping. All numbers are in eV.

Sample	t	t'	t''	$t_\perp$	$\Delta\varepsilon$
OD69.0K	0.40	0.090	0.045	0.082	0.431
UD77.0K	0.39	0.076	0.034	0.097	0.304
OD56.0K	0.40	0.092	0.047	0.081	0.449
OD74.3K	0.40	0.089	0.044	0.084	0.422
OP92.2K	0.39	0.082	0.039	0.090	0.361
UD83.0K	0.39	0.077	0.035	0.096	0.317

The first model we consider is the conventional BCS model. In this case the self-energy reads:

$$\Sigma^{(1)}(\boldsymbol{k},\omega) = \frac{|\Delta_{\boldsymbol{k}}|^2}{\omega + i\Gamma + \varepsilon_{\boldsymbol{k}}}, \tag{4}$$

where the gap has $d_{x^2-y^2}$ symmetry: $\Delta_{\boldsymbol{k}} = \frac{1}{2}\Delta_0(\cos k_x - \cos k_y)$. The only free parameter, Δ_0, is adjusted to the experimental data. In general, the optimum Δ_0 in our models can be determined with meV resolution from the comparison to the experimental data.

In the second model, we follow an attempt to fit ARPES measurements[24] by complementing the BCS model with a phenomenological $\boldsymbol{k}$-independent self-energy $\Sigma_0(\omega)$. At low energy, $\Sigma_0(\omega)$ has a marginal Fermi liquid form:

$$\Sigma_0(\omega) = -\lambda\omega - i\sqrt{(\alpha_0\omega)^2 + (\beta_0 k_{\mathrm{B}} T)^2}. \tag{5}$$

Good agreement with ARPES was found with the parameters $\lambda = 1$, $\alpha_0 = 2$, and $\beta_0 = 4$.[24,30–33] The complete self-energy including the superconducting gap is

$$\Sigma^{(2)}(\boldsymbol{k},\omega) = \Sigma_0(\omega) + \frac{|\Delta_{\boldsymbol{k}}|^2}{\omega + i\Gamma + \varepsilon_{\boldsymbol{k}} - \Sigma_0(\omega)}. \tag{6}$$

Equation (6) can be recast in a form similar to Eq. (4), with the bare dispersion $\varepsilon_{\boldsymbol{k}}$ and gap $\Delta_{\boldsymbol{k}}$ renormalized to $c\varepsilon_{\boldsymbol{k}}$ and $c\Delta_{\boldsymbol{k}}$, respectively, and the lifetime broadening Γ replaced by

$\Gamma - c\,\mathrm{Im}\,\Sigma_0(\omega)$ with $c=(1+\lambda)^{-1}$. We will use Eq. (6) to check if the self-energy inferred from ARPES is compatible with the STS data.

Finally, the third model we consider accounts for the possible interaction of the quasiparticles with a collective mode. Such a mode was indeed observed in BSCCO by neutron scattering, with momentum centered at (π,π).[25] It appears at an energy $\Omega \approx 5.4 k_B T_c$,[26] and is characterized by a correlation length $\xi \lesssim 2$ in lattice units (we will take $\xi=2$ in our simulations). The interaction of this mode with the electrons was described theoretically in Ref. 27, and involves a coupling constant g for which we choose the value $g=0.65$ eV. The self-energy entering Eq. (2) is

$$\Sigma^{(3)}(\boldsymbol{k},\omega)=\Sigma_{11}(\boldsymbol{k},\omega)+\frac{|\Delta_{\boldsymbol{k}}+\Sigma_{12}(\boldsymbol{k},\omega)|^2}{\omega+i\Gamma+\varepsilon_{\boldsymbol{k}}-\Sigma_{22}(\boldsymbol{k},\omega)}. \quad (7)$$

The components Σ_{ij} are a convolution of the bare BCS propagator (in Nambu representation) with the spin susceptibility. The latter is represented by a simple analytical function which approximates the neutron measurements. We refer the reader to Ref. 27 for further details.

Very little is known about the actual $\boldsymbol{k}$-dependence of the tunneling matrix element, although band calculations suggest that it is anisotropic with a shape corresponding to the dispersion of the bilayer splitting,[34] i.e. $(\cos k_x - \cos k_y)^2$. Such a matrix element would prohibit tunneling into the nodal direction (π,π) and would highlight the region $(\pi,0)$ of the van Hove singularities. We will consider the two limiting cases of a completely isotropic $T_s=T_0$ and anisotropic $T_d=T_0(\cos k_x-\cos k_y)$ matrix element, as well as admixtures of the form $|T_{\boldsymbol{k}}|^2=\alpha|T_s|^2+(1-\alpha)|T_d|^2$.

For each model we calculate the differential tunneling conductance using Eq. (1) and a 1024×1024 mesh of $\boldsymbol{k}$ points. The temperature is set to 4.2 K. The experimental energy resolution is simulated by filtering the data with a Gaussian of width 1 meV. Finally, unless stated otherwise, the calculated spectra are normalized to the total spectral weight of the experimental data over the energy range from -300 to $+300$ meV.

III. RESULTS AND DISCUSSION

A. BCS model

To compare the calculated spectra with experimental results over a wide doping range, we use low-temperature (4.2 K) data of Renner *et al.*[1] The results of the BCS model, with an isotropic matrix element, are shown in Fig. 1. The agreement at subgap energies is good, except for OD74.3K where the spectral weight is somewhat underestimated. The (calculated and experimental) spectra show the V-shape at zero bias typical for a *d*-wave order parameter. At higher energies, however, the model misses the dip-hump feature, which is most pronounced in the optimally doped and underdoped spectra at -60 to -100 meV, and the model generally presents too sharp structures. In particular, the van Hove singularities of the A and B bands show up unrenormalized in the spectra while no such singularities exist in the experimental curves. None of these discrepancies can be reduced by the inclusion of an anisotropic matrix element, which would suppress spectral weight below the gap energy and raise the van Hove singularities even more. Nevertheless, with this first approach we can draw some conclusions which remain valid for the more sophisticated models discussed below.

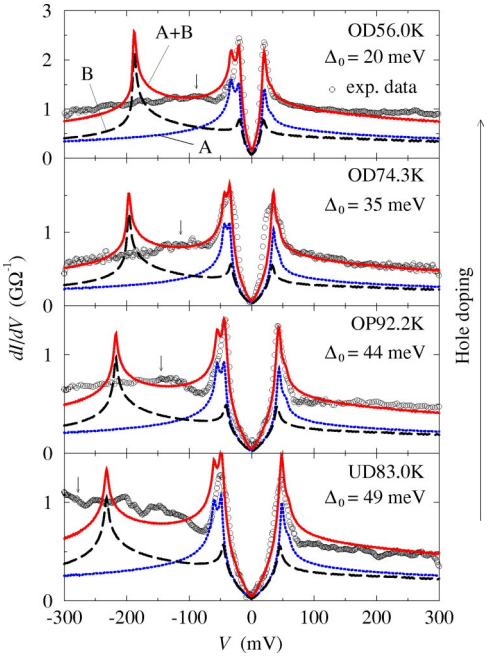

FIG. 1. Tunneling spectra in the conventional BCS model, with a *d*-wave superconducting gap and an isotropic matrix element. The contributions of the A and B bands are shown separately, and their sum should be compared to the experimental data (circles). The arrows roughly indicate the maximum of the broad feature in the background (see the text).

From the difference between the A and B bands, it becomes clear that most of the weight of the coherence peaks in the tunneling spectra is related to the van Hove singularity of the A band, which lies close to the Fermi level. The presence of the van Hove singularity in the coherence peaks explains their unusual height.[15] Note, however, that without the B band the peaks would become too high (with respect to the background) to fit the experimental data. The van Hove singularity also explains why the peak at negative bias is generally a bit higher than the one at positive bias.

In general, we observe that the van Hove singularity of the A band remains close to the Fermi level (integrated in the coherence peaks) for all doping levels. The van Hove singularity of the B band, however, moves to higher binding energy with underdoping. This shift is related to the combined effects of increasing gap and increasing $t_\perp$ with underdoping. It is in qualitative agreement with the behavior observed in the background of the experimental data:[1,2] on going from overdoped to underdoped, the background of the spectra becomes more asymmetric. One can distinguish a very broad feature moving away from the Fermi level with underdoping. In fact, we have shown that this background can be fitted very well by a broadened van Hove singularity at energies consistent with the doping level, in a rigid single-band

picture.[35] These energies are indicated by arrows in Fig. 1. In the present calculation, however, the van Hove peaks are located at different energies.

Summarizing this discussion, the tunneling spectra are consistent with a sharp van Hove singularity just below the Fermi level, and a very broad van Hove singularity moving to higher binding energy with underdoping. Apart from the dip-hump feature, the questions left open by the BCS model are the precise energy shift of the van Hove singularity of the bonding band, as well as the mechanism of its broadening.

B. Comparison of tunneling and ARPES

The absence of a sharp van Hove singularity of the B band in the tunneling spectra is a clear indication that one should go beyond the bare BCS DOS to explain all features in the spectra. In principle, it should be possible to take spectral functions directly from ARPES data and sum them to compare to the tunneling results. However, this is complicated by the strong influence of matrix elements on the photoemission spectra (see, e.g., Ref. 30) and of the background in the ARPES data. We therefore rely on the phenomenological model of the spectral function at low energy described above [with self-energy Eq. (6)]. This description crudely includes the effects of correlation in the marginal Fermi liquid self-energy $\Sigma_0(\omega)$. With such an approach we can first directly compare tunneling and ARPES, and also study the ability of the marginal Fermi liquid model to account for tunneling data.

The ARPES data could be fitted using Eq. (6) with $\alpha_0 = 2$. In Fig. 2 we compare the calculations for $\alpha_0 = 2$ to experimental tunneling data. Note that the energy scale is a factor 2 smaller than in Figs. 1 and 3. As can be seen, the calculated curves (dotted lines) do not fit the experimental data at all. In particular, the V-shape of the spectra at low energy is too narrow. One might expect that the excess spectral weight in the gap can be suppressed by an anisotropic matrix element. However, as shown by the dashed lines, this is not the case. The reason is that the low-energy spectral weight is dominated by the marginal Fermi liquid self-energy, and not by the gap function.

Surprisingly, a good fit can be obtained by an order of magnitude reduction of α_0, to $\alpha_0 = 0.2$, assuming an isotropic matrix element. This difference in $\Sigma_0'' = \mathrm{Im}\,\Sigma_0$ for ARPES and tunneling suggests, not for the first time,[36] that the scattering rate in ARPES is considerably higher than in tunneling. The explanation for this remarkable difference goes beyond our current understanding of ARPES and tunneling.

The van Hove singularity of the B band is shifted closer to the Fermi level as a result of band renormalization by a factor $(1+\lambda)^{-1}$. Furthermore, the energy dependence of Σ_0'' leads to a broadening which is more important at higher energies. At negative bias this results in a coherence peak followed by the broadened van Hove singularity of the B band. However, the energy shift of this van Hove singularity as a function of doping is too small compared to the broad feature in the background (see Sec. III A). Of course one can question the validity of the assumption $\mathrm{Re}\,\Sigma_0 = -\lambda\omega$ at energies above ~ 50 meV,[32] meaning that the van Hove singularity of the B band is at too low binding energy in our simulations. Taking this into account would probably lead to a better agreement with the broad maximum in the background, shifting away from the Fermi level with underdoping. However, this behavior is inconsistent with the sharpness of the dip when the van Hove singularity is at much higher binding energy than the dip (as is specifically the case for the optimally and underdoped samples).

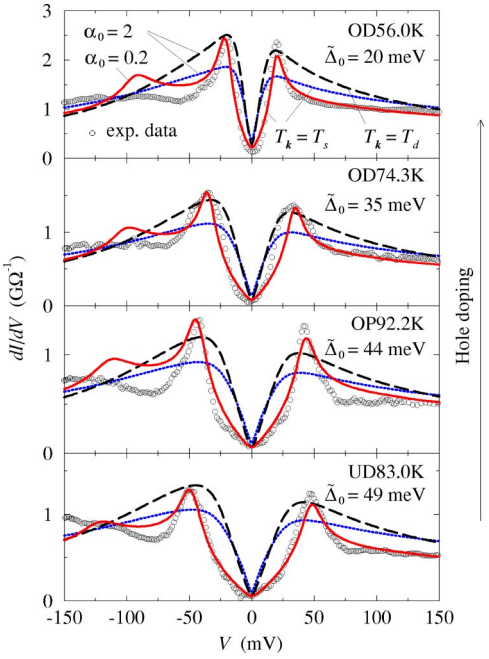

FIG. 2. Tunneling spectra calculated using the phenomenological self-energy Eq. (6) and compared to the experimental data (circles). Spectra are shown for $\alpha_0 = 2$ with the isotropic (dotted curve) and anisotropic (dashed curve) matrix element, the latter highlighting the $(\pi,0)$ region of the Brillouin zone, and for $\alpha_0 = 0.2$ with the isotropic matrix element. The two curves for $\alpha_0 = 2$ are normalized to the spectral weight between -300 and $+300$ meV, while the curve for $\alpha = 0.2$ is normalized to the peak height. $\tilde{\Delta}_0 = (1+\lambda)^{-1}\Delta_0$ is the renormalized gap value. All spectra are for $\lambda = 1$ and $\beta_0 = 4$.

C. Coupling to a collective mode

So far, it has not been established whether the coupling of quasiparticles to the collective mode observed in neutron scattering experiments, is sufficient to have a sizable influence on the spectral functions[37] or not.[38] In the following analysis we assume it is, and verify to which extent the tunneling spectra are consistent with neutron scattering data on the (π,π) mode.

In this model [Eq. (7)], the main effect of the resonant mode is to enhance the imaginary part Σ'' of the self energy between the energies $\varepsilon_1 = -\Omega - \Delta_0$ and $\varepsilon_2 = -\Omega - \sqrt{\varepsilon_{\mathrm{vHs}}^2 + \Delta_0^2}$, where $\varepsilon_{\mathrm{vHs}}$ is the band energy at the $(\pi,0)$ point.[27] A similar effect, although much smaller, exists at positive bias. The numerical results are displayed in Fig. 3. Focusing first on curves A, which represent the DOS of the A band, we notice the sharp coherence peaks. The energy of the

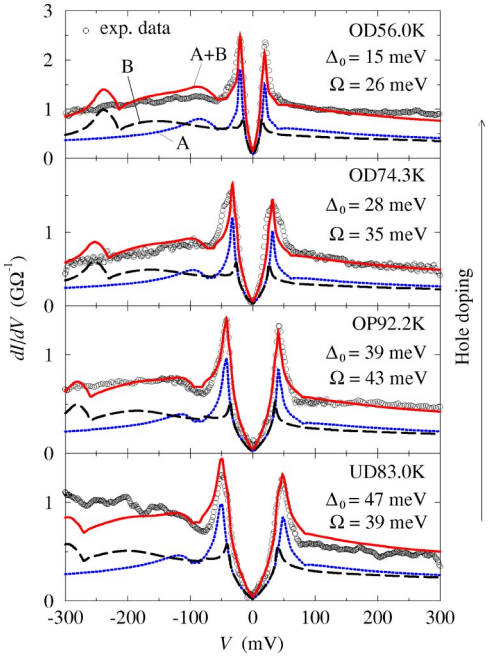

FIG. 3. Tunneling spectra including interaction with a bosonic mode at wave vector (π,π) and energy $\Omega=5.4k_BT_c$. The coupling constant and correlation length are $g=0.65$ eV and $\xi=2$, respectively. The superconducting gap has *d*-wave symmetry and the tunneling matrix element is isotropic. The contributions of the A and B bands are shown separately, and their sum should be compared to the experimental data.

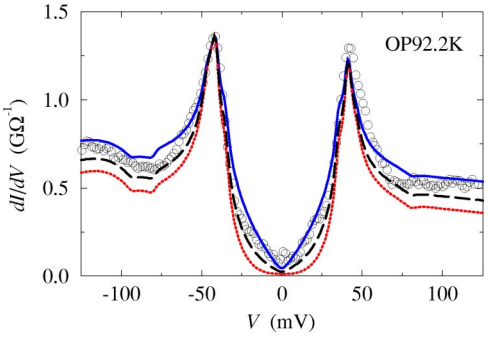

FIG. 4. Comparison of the STS spectra including the coupling to the (π,π) mode, calculated with different matrix elements. $\Delta_0=39$ meV, as in Fig. 3. The continued line corresponds to the isotropic case $T_{\mathbf{k}}=T_s$, the dotted line to the anisotropic case $T_{\mathbf{k}}=T_d$, and the dashed line to a partly anisotropic matrix element $|T_{\mathbf{k}}|^2=0.4|T_s|^2+0.6|T_d|^2$. The spectra have been normalized to the peak height at -44 meV.

latter is a combination of the gap value and the van Hove singularity which, as in the previous models, lies very close to the gap edges, and contributes much to the total spectral weight of the coherence peaks. Furthermore, it is crucial for the creation of the dip-hump feature, below the coherence peak at negative bias. The width of the dip corresponds to the energy interval between ε_1 and ε_2 where Σ'' is enhanced. Below the dip, there is a hump resulting from the scattering out of the above energy interval. The mode energy deferred from neutron scattering[25,26] results in a reasonable agreement with the dip in the tunneling spectra (also see Ref. 4). However, we caution that its shape is more dependent on the precise values of Δ_0 and $\varepsilon_{\mathrm{vHs}}$ than on the mode energy itself. Furthermore, for the optimally and underdoped samples the calculated dip is at slightly higher binding energy than in the experimental data, suggesting that the mode energy is smaller than determined from neutron scattering. Finally, the depth of the dip in the experimental data indicates an increasing coupling constant g with underdoping.

Let us now turn to the DOS of the B band. Here the coherence peaks are small and occur at Δ_0. The energy interval between ε_1 and ε_2 is much larger than for the A band, and below ε_2 we see again a hump structure. The van Hove peak of the B band now appears inside the dip energy range as a very broad maximum. Comparing the curves at different dopings, we find that the broad maximum shifts away from the Fermi level with underdoping. Though this shift is smaller than suggested by experiment, it is in qualitative agreement with experiment. The only disagreement occurs at higher binding energies, where the hump coming from the B band is not observed in experiment. This hump is probably smeared out by coupling to the continuum of spin excitations at higher energies,[39] not taken into account here.

In Fig. 4 we compare experimental data to spectra calculated using different matrix elements. It is clear that the experimental spectrum at low bias shows the V-shape typical for a *d*-wave superconductor, and *not* the U-shape expected for tunneling with a completely anisotropic matrix element. Though some anisotropy is not to be excluded, the tunneling spectra are thus more consistent with isotropic than with anisotropic tunneling matrix elements that suppress all states along the diagonals of the Brillouin zone. This conclusion is independent of the exact model chosen here (it can also be witnessed from, for example, the bare DOS in Fig. 1), and only dependent on the assumption of the *d*-wave symmetry of the order parameter and a small imaginary part of the self-energy at low energy.

IV. SUMMARY

We have modeled scanning tunneling spectra of BSCCO including *d*-wave BCS superconductivity, band dispersions based on recent ARPES data (with bilayer splitting), and isotropic as well as anisotropic tunneling matrix elements. In addition to this, we have compared tunneling spectra to ARPES data via a phenomenological marginal Fermi liquid approach. In a third model, we have taken into account coupling of quasiparticles to a collective mode with momentum (π,π). All numerical results have been compared to experimental data over a large doping range.

The simple *d*-wave BCS model reproduces several general characteristics of the experimental tunneling spectra, but fails to account for salient features like the dip-hump structure and the absence of a sharp van Hove singularity from the bonding band. The comparison between tunneling and ARPES suggests a much longer lifetime in tunneling experiments than in ARPES: using the marginal Fermi liquid approach, the shape of the coherence peaks in tunneling spectra is correctly reproduced, but only if the lifetime is taken an

order of magnitude larger than inferred from ARPES data, an observation that remains to be explained. This model, specified for low energy, does not lead to a satisfactory description of the dip-hump structure and the asymmetric background as a function of doping. Important improvement is obtained by including the interaction of quasiparticles with a collective mode. With parameters inferred from neutron scattering experiments, reasonable agreement with the tunneling spectra is found, though the energy of the mode may be slightly overestimated for the optimally and underdoped samples.

In general, the tunneling spectra are consistent with the presence of a sharp van Hove singularity (of the antibonding band) integrated in the coherence peaks, and a broad van Hove singularity (of the bonding band) in the background, shifting away from the Fermi level with underdoping. These van Hove singularities can be held responsible for the asymmetry in tunneling spectra with respect to zero bias. The broadening of the bonding band van Hove singularity can be largely attributed to the collective mode. This mode also leads to a dip-hump feature in the spectra, which is more pronounced in the underdoped than in the overdoped samples. The exact shape and depth, however, also depend on van Hove singularity of the antibonding band and on the superconducting gap.

Finally, the shape of the spectra at low-bias voltage is indicative of an isotropic tunneling matrix element. We conclude that the tunneling matrix element does not have a strong dependence on the (in-plane) wave vector. Tunneling spectroscopy therefore probes states along the whole Fermi surface, including the diagonals of the Brillouin zone.

ACKNOWLEDGMENTS

We acknowledge A. A. Manuel for programming assistance, Ch. Renner for sharing his long experience in tunneling spectroscopy, and G. A. Sawatzky for his repeatedly questioning about tunneling matrix elements. This work was supported by the Swiss National Science Foundation.

*Present address: M. E. Müller Institute for Structural Biology, Biozentrum, University of Basel, Klingelbergstrasse 70, CH-4056 Basel, Switzerland.

Electronic address: Bart.Hoogenboom@unibas.ch

†Deceased.

[1] Ch. Renner, B. Revaz, J.-Y. Genoud, K. Kadowaki, and Ø. Fischer, Phys. Rev. Lett. **80**, 149 (1998).

[2] N. Miyakawa, J. F. Zasadzinski, L. Ozyuzer, P. Guptasarma, D. G. Hinks, C. Kendziora, and K. E. Gray, Phys. Rev. Lett. **83**, 1018 (1999).

[3] E. W. Hudson, S. H. Pan, A. K. Gupta, K.-W. Ng, and J. C. Davis, Science **285**, 88 (1999).

[4] J. F. Zasadzinski, L. Ozyuzer, N. Miyakawa, K. E. Gray, D. G. Hinks, and C. Kendziora, Phys. Rev. Lett. **87**, 067005 (2001).

[5] S. H. Pan, J. P. O'Neal, R. L. Badzey, C. Chamon, H. Ding, J. R. Engelbrecht, Z. Wang, H. Eisaki, S. Uchida, A. K. Gupta, K.-W. Ng, E. W. Hudson, K. M. Lang, and J. C. Davis, Nature (London) **413**, 282 (2001).

[6] B. W. Hoogenboom, K. Kadowaki, B. Revaz, M. Li, Ch. Renner, and Ø. Fischer, Phys. Rev. Lett. **87**, 267001 (2001).

[7] J. E. Hoffman, E. W. Hudson, K. M. Lang, V. Madhavan, S. H. Pan, H. Eisaki, S. Uchida, and J. C. Davis, Science **295**, 466 (2002).

[8] S. Misra, S. Oh, D. J. Hornbaker, T. DiLuccio, J. N. Eckstein, and A. Yazdani, Phys. Rev. Lett. **89**, 087002 (2002).

[9] S. Kaneko, N. Nishida, K. Mochiku, and K. Kadowaki, Physica C **298**, 105 (1998).

[10] S. Matsuura, T. Taneda, W. Yamaguchi, H. Sugawara, T. Hasegawa, and K. Kitazawa, Physica C **300**, 26 (1998).

[11] A. Matsuda, S. Sugita, and T. Watanabe, Phys. Rev. B **60**, 1377 (1999).

[12] G. D. Mahan, *Many-Particle Physics*, 2nd ed. (Plenum Press, New York, 1983).

[13] W. A. Harrison, Phys. Rev. **123**, 85 (1961).

[14] J. Bok and J. Bouvier, Physica C **274**, 1 (1997).

[15] J. Y. T. Wei, C. C. Tsuei, P. J. M. van Bentum, Q. Xiong, C. W. Chu, and M. K. Wu, Phys. Rev. B **57**, 3650 (1998).

[16] J. E. Hirsch, Phys. Rev. B **59**, 11 962 (1999).

[17] T. Cren, D. Roditchev, W. Sacks, J. Klein, J.-B. Moussy, C. Deville-Cavellin, and M. Laguës, Phys. Rev. Lett. **84**, 147 (2000).

[18] K. Kouznetsov and L. Coffey, Phys. Rev. B **54**, 3617 (1996).

[19] Z. Yusof, J. F. Zasadzinski, L. Coffey, and N. Miyakawa, Phys. Rev. B **58**, 514 (1998).

[20] M. Franz and Z. Tešanović, Phys. Rev. B **60**, 3581 (1999).

[21] D. L. Feng, N. P. Armitage, D. H. Lu, A. Damascelli, J. P. Hu, P. Bogdanov, A. Lanzara, F. Ronning, K. M. Shen, H. Eisaki, C. Kim, J.-i. Shimoyama, K. Kishio, and Z.-X. Shen, Phys. Rev. Lett. **86**, 5550 (2001).

[22] Y.-D. Chuang, A. D. Gromko, A. Fedorov, Y. Aiura, K. Oka, Y. Ando, H. Eisaki, S. I. Uchida, and D. S. Dessau, Phys. Rev. Lett. **87**, 117002 (2001).

[23] A. A. Kordyuk, S. V. Borisenko, M. S. Golden, S. Legner, K. A. Nenkov, M. Knupfer, J. Fink, H. Berger, L. Forró, and R. Follath, Phys. Rev. B **66**, 014502 (2002).

[24] A. A. Kordyuk, S. V. Borisenko, M. Knupfer, and J. Fink, Phys. Rev. B **67**, 064504 (2003).

[25] H. F. Fong, P. Bourges, Y. Sidis, L. P. Regnault, A. Ivanov, G. D. Gu, N. Koshizuka, and B. Keimer, Nature (London) **398**, 588 (1999).

[26] H. He, Y. Sidis, P. Bourges, G. D. Gu, A. Ivanov, N. Koshizuka, B. Liang, C. T. Lin, L. P. Regnault, E. Schoenherr, and B. Keimer, Phys. Rev. Lett. **86**, 1610 (2001).

[27] M. Eschrig and M. R. Norman, Phys. Rev. Lett. **85**, 3261 (2000).

[28] S. V. Borisenko, A. A. Kordyuk, T. K. Kim, S. Legner, K. A. Nenkov, M. Knupfer, M. S. Golden, J. Fink, H. Berger, and R. Follath, Phys. Rev. B **66**, 140509(R) (2002).

[29] For all samples, the doping p was determined from T_c, assuming the generic $T_c - p$ relation given in: J. L. Tallon, C. Bernhard, H. Shaked, R. L. Hitterman, and J. D. Jorgensen, Phys. Rev. B **51**, 12 911 (1995).

[30] A. A. Kordyuk, S. V. Borisenko, T. K. Kim, K. A. Nenkov, M. Knupfer, J. Fink, M. S. Golden, H. Berger, and R. Follath, Phys. Rev. Lett. **89**, 077003 (2002).

[31] A. Lanzara, P. V. Bogdanov, X. J. Zhou, S. A. Kellar, D. L. Feng, E. D. Lu, T. Yoshida, H. Eisaki, A. Fujimori, K. Kishio, J.-I. Shimoyama, T. Noda, S. Uchida, Z. Hussain, and Z.-X. Shen, Nature (London) **412**, 510 (2001).

[32] P. D. Johnson, T. Valla, A. V. Fedorov, Z. Yusof, B. O. Wells, Q. Li, A. R. Moodenbaugh, G. D. Gu, N. Koshizuka, C. Kendziora, S. Jian, and D. G. Hinks, Phys. Rev. Lett. **87**, 177007 (2001).

[33] A. D. Gromko, Y.-D. Chuang, A. V. Fedorov, Y. Aiura, Y. Yamaguchi, K. Oka, Y. Ando, and D. S. Dessau, cond-mat/0205385 (unpublished).

[34] O. K. Andersen, A. I. Liechtenstein, O. Jepsen, and F. Paulsen, J. Phys. Chem. Solids **56**, 1573 (1995).

[35] B. W. Hoogenboom, Ph.D. thesis, University of Geneva, 2002.

[36] M. Franz and A. J. Millis, Phys. Rev. B **58**, 14 572 (1998).

[37] A. Abanov, A. V. Chubukov, M. Eschrig, M. R. Norman, and J. Schmalian, Phys. Rev. Lett. **89**, 177002 (2002).

[38] H.-Y. Kee, S. A. Kivelson, and G. Aeppli, Phys. Rev. Lett. **88**, 257002 (2002).

[39] M. Eschrig and M. R. Norman, cond-mat/0202083 (unpublished).